

## P4.12 RAPID-SCAN OBSERVATIONS OF A BOW ECHO STORM WITH A DUAL-POLARIZATION WSR-88D

MATTHEW R. KUMJIAN\* AND ALEXANDER V. RYZHKOV

*Cooperative Institute for Mesoscale Meteorological Studies, University of Oklahoma, and NOAA/OAR National Severe Storms Laboratory, Norman, OK*

### 1. INTRODUCTION

For the first time a polarimetric WSR-88D radar is used to collect data using a rapid scanning strategy for a severe bow echo storm. Previous studies employing dual-polarization radar to analyze mesoscale convective systems (MCSs) have focused on the microphysics of the convective region (e.g., Meischner et al. 1991), the stratiform precipitation region (e.g., Zrnić et al. 1993), or the overall precipitation characteristics of such systems (e.g., Ryzhkov and Zrnić 1994). Additionally, these previous studies use conventional radar volume coverage patterns that require between 5 and 7 minutes to complete. This study will focus on the formation of a rear inflow jet (RIJ; e.g., Smull and Houze 1987) and the ensuing evolution of the polarimetric variables.

The next two subsections discuss brief overviews of the MCS event and the data collection methodology. The data are presented in section 2. Section 3 discusses these observations and provides a conceptual analysis of the polarimetric variable evolution. The main conclusions are summarized in section 4.

#### 1.1. Event Overview

On 26 May 2008, an upper-level trough was lifting out over the Great Plains. In Oklahoma, surface temperatures reached about 30 °C while dewpoints across the state were between 20 – 22 °C. The atmosphere was unstable, with about 2000 J kg<sup>-1</sup> of CAPE present on the 00 UTC Norman (OUN) sounding (Fig. 1). Storms initiated along the dryline in the eastern Texas panhandle in the afternoon. After sunset, a south-southeasterly 15 m s<sup>-1</sup> low-level jet developed and the discrete storms congealed into a MCS that re-aligned itself into the low-level shear. The instability and shear in the environment were marginally conducive to bow echo formation according to the criteria suggested by Weisman (1992) and Bluestein (1993).

#### 1.2. Data Collection

The data were collected by the research polarimetric prototype WSR-88D in Norman, Oklahoma (KOUN). Starting at 2230 UTC, KOUN collected data in a super-resolution (0.5° azimuthal sampling) version of the standard National Weather Service volume coverage pattern (VCP). The rapid-scan data collection began at 0643 UTC. Data were collected in a 60° sector centered on 300°. The details of this scanning regime are provided in Table 1. The conventional super-resolution VCP was resumed at 0658

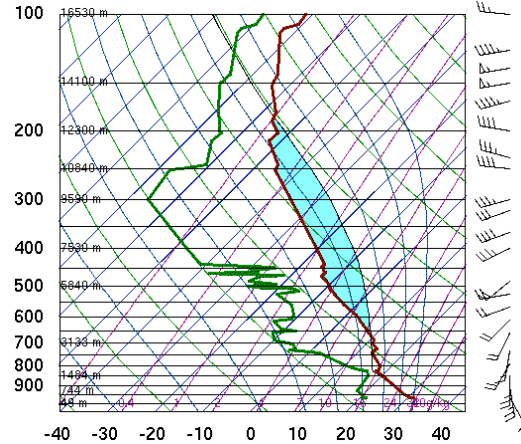


Fig. 1: Observed sounding from OUN on 27 May, 2008 at 00 UTC. The red line is temperature (°C) and the green line is dewpoint temperature. The blue shading represents the surface-based CAPE.

<b>Azimuthal Resolution</b>	1°
<b>Range Resolution</b>	250 m
<b>Nyquist Velocity</b>	± 35 m s <sup>-1</sup>
<b>Elevation angles (20)</b>	0.3°, 0.8°, 1.3°, 1.8°, 2.3°, 2.8°, 3.5°, 4.2°, 5.0°, 5.9°, 6.9°, 8.1°, 9.2°, 10.6°, 12.0°, 13.6°, 15.3°, 17.6°, 19.6°, 22.1°
<b>Update time</b>	94 s

Table 1: Details of the scanning regime used for the rapid-scanning of the bow echo.

UTC. The 15 minute period of rapid updates captured the evolution of the RIJ and subsequent bowing of the MCS. This is seen in Figure 2, which shows the conventional super-resolution PPI scan just before and just after the period of sector scans.

### 2. RAPID-SCAN DATA

The rapid scan data were collected during the times between the two images shown in Figure 2, centered at an azimuth of 300°. This corresponds with the center of part of the line, approximately where the apex of the subsequent bow forms. A series of Z<sub>DR</sub> and Z<sub>H</sub> observations from every other scan reveals the evolution of the system (Fig. 3). It is evident that the Z<sub>DR</sub> field has more variability than the Z<sub>H</sub> field over the time period displayed in the figure. Also, as Z<sub>H</sub> decreases at the rear of the storm, Z<sub>DR</sub> increases. Of note is the developing cell at the leading edge of the storm (centered at about x = -40 km, y = 10 km at the time of the first observation). Though reflectivity is generally about 40 dBZ,

\*Corresponding author address: Matthew R. Kumjian, 120 David L. Boren Blvd., National Weather Center Suite 4900, Norman, OK 73072. Email: matthew.kumjian@noaa.gov

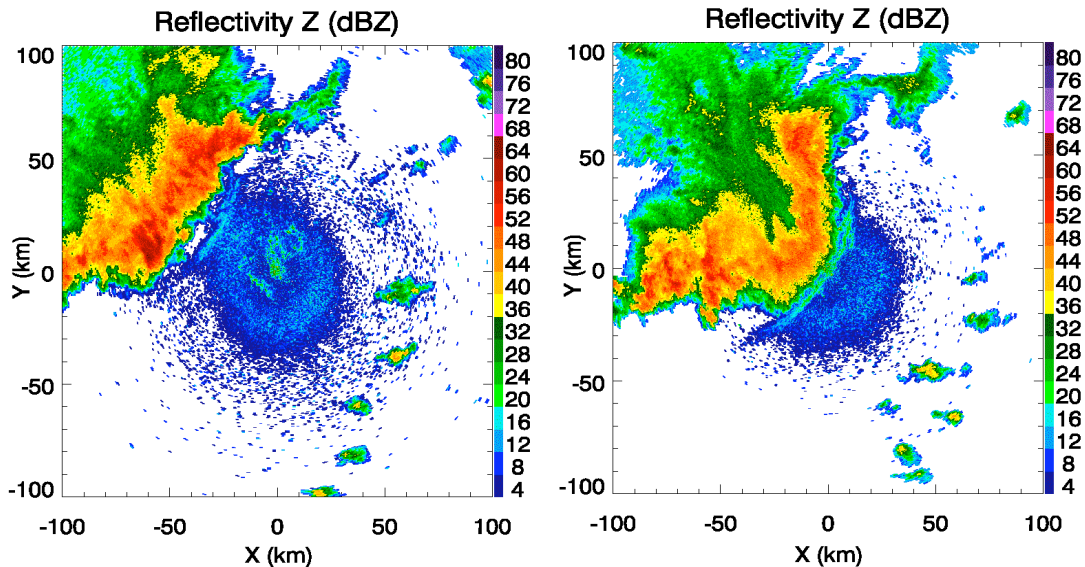


Fig. 2: Conventional  $0.8^\circ$  PPI super-resolution scans of radar reflectivity factor  $Z_H$  (dBZ) just prior to (0642 UTC, on the left) and just after (0658 UTC, on the right) the rapid scan data collection period.

the measured  $Z_{DR}$  approaches 4 dB, indicative of a fairly skewed DSD with a preponderance of larger drops. This is likely a result of size sorting by the developing updraft and vertical shear (Kumjian and Ryzhkov 2009). With time, the cell merges with the main body of the convective line.

The evolution of the Doppler velocity field reveals an area of strong divergence near the front of the system (Fig. 4). Over time, the inbound velocity maxima increases in magnitude at low-levels, likely a manifestation of the high momentum air aloft decreasing as it approaches the front of the storm. The largest inbound velocities at the  $0.8^\circ$  elevation level are about  $35 - 40 \text{ m s}^{-1}$ , which would be considered severe if at the surface. The divergence is located just in front of a strong  $Z_H$  core ( $> 60 \text{ dBZ}$ ). Collocated with this high- $Z_H$  core is very high  $K_{DP}$  ( $> 3 \text{ deg km}^{-1}$ ), high  $Z_{DR}$  ( $> 3 \text{ dB}$ ), and  $\rho_{HV} < 0.975$  (Fig. 5). This indicates the presence of a mixture of melting hailstones and heavy rain, both of which will contribute to negative buoyancy, which can enhance the downdraft and divergence signatures. Also of note in Fig. 5 is that the high  $Z_{DR}$  is also found along the front edge of the MCS where  $K_{DP}$  is quite low ( $< 0.5 \text{ deg km}^{-1}$ ) and  $Z_H$  values are modest. This is indicative of size sorting, as mentioned above. Towards the end of the observation period, the magnitudes of the velocity and divergence signatures decrease as a result of the storm weakening.

### 3. ANALYSIS AND DISCUSSION

There have been many conceptual models for squall lines presented in the literature (e.g., Smull and Houze 1987; Houze et al. 1989; Schuur et al. 1991; Biggerstaff and Houze 1991; Houze 1993). One of the basic components of each of these models is the ascending front-to-rear current of air originating with the convective updrafts at the leading edge of the storm. The ascending front-to-rear flow is associated with convection and thus is positively buoyant. Precipitation falling into subsaturated air chills the air, producing a negatively buoyant cold pool at the surface beneath this front-to-rear flow. Between these regions is a pronounced, mainly

hydrostatic negative pressure perturbation. The negative pressure perturbation is largest in magnitude closer to the strongest convection near the front of the storm. Thus, the resulting pressure gradient force accelerates dry, midlevel environmental air from behind the storm towards the leading edge. Dynamic effects can also enhance this pressure perturbation gradient force. A perturbation low is often found at the head of the cold pool, where a local horizontal vorticity maximum occurs. Centrifugal forcing associated with this vorticity results in a negative pressure perturbation (see Fovell and Ogura 1988).

As hydrometeors fall into this rear-to-front current, they may evaporate, melt, or sublimate, chilling the unsaturated air and causing the current to descend (e.g., Lafore and Moncrieff 1989). The rear inflow current or RIJ enters the stratiform region just above the melting level, whereupon it subsides through the layer and reaches the ground beneath the convective cells. There it may reinforce convergence at the leading gust front (evident as a thin line ahead of the storm in Fig. 2). The erosion of  $Z_H$  and  $K_{DP}$  and the collocated increase in  $Z_{DR}$  presented in the previous section are indicative of evaporation of hydrometeors falling into the subsaturated RIJ. The erosion of  $Z_H$  can be attributed to the evaporation, which causes a decrease in number concentration of particles as smaller raindrops evaporate as well as the overall decrease in size of all raindrops. The resulting intrusion of low  $Z_H$  into the rear of the storm is a commonly observed manifestation of the RIJ (e.g., Smull and Houze 1987).  $K_{DP}$  is often quite similar to  $Z_H$  in rain; however,  $K_{DP}$  is more sensitive to smaller drop sizes than  $Z_H$  (because  $K_{DP} \sim D^{4.24}$  whereas  $Z_H \sim D^6$ ). Thus, the evaporative loss of smaller drops causes  $K_{DP}$  to erode in a fashion similar to  $Z_H$ . However, it appears as if the erosion of  $K_{DP}$  is more pronounced or more readily apparent than the erosion of  $Z_H$ , likely due to this greater sensitivity to smaller drops (Fig. 6). Simple modeling results from Kumjian and Ryzhkov (2008) indicate that for given environmental conditions, the erosion in  $K_{DP}$  due to evaporation increases with increasing rainfall

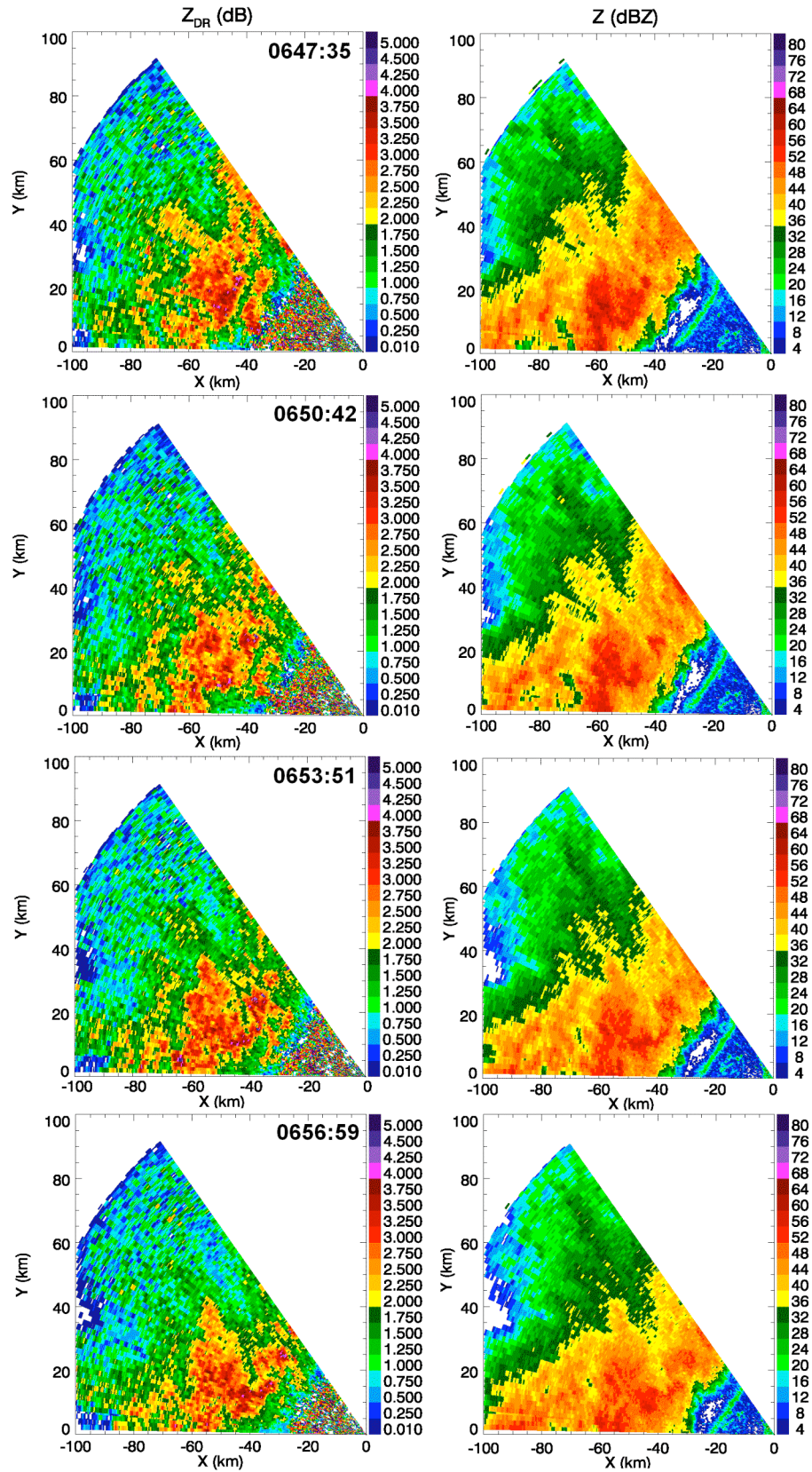


Fig. 3: Evolution of  $Z_{DR}$  (left) and  $Z_H$  (right) over the rapid scan collection period, taken at an elevation of  $0.8^\circ$ . The time of the sector scan (UTC) is given in the  $Z_{DR}$  panel.

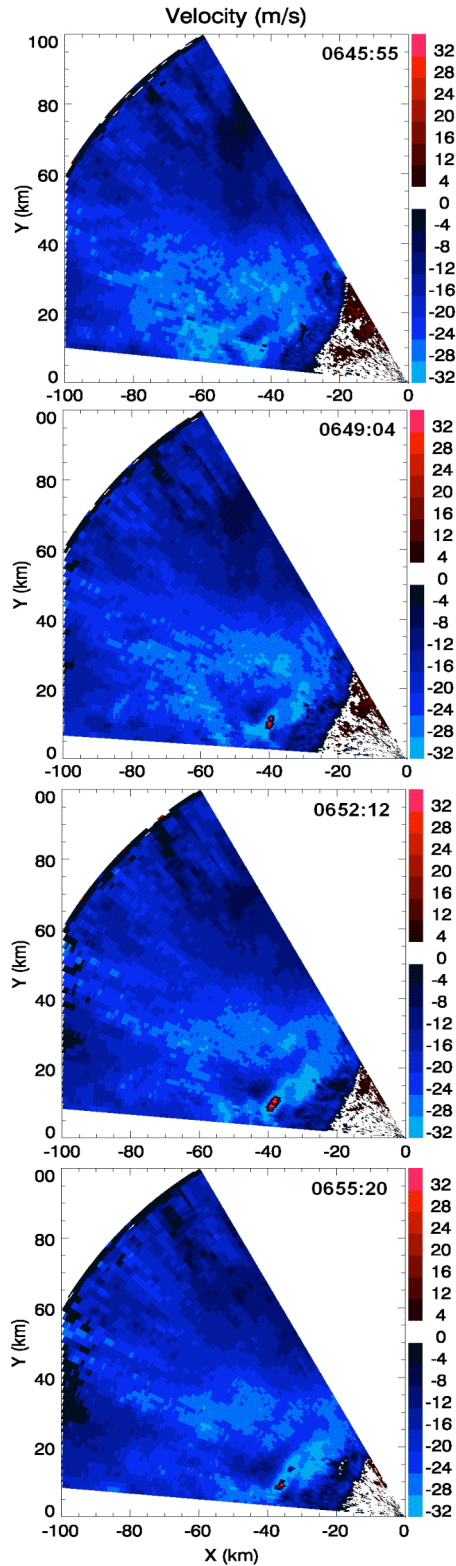


Fig. 4: Base Doppler velocity data during the rapid scan observational period. The strong divergence signature is located at about  $x = -40$  km,  $y = 10$  km. The time (UTC) is plotted in each panel. Data come from the  $0.8^\circ$  elevation angle.

rate, while concurrently the change in  $Z_H$  decreases (Fig. 7). The details of the evaporation model can be found in that paper. As the RIJ penetrates into regions of higher  $Z_H$ , indicative of heavier rainfall, the difference between the erosion of  $Z_H$  and  $K_{DP}$  should become even more apparent. Thus, forecasters may use the erosion of  $K_{DP}$  at the back edge of the storm to increase lead times for warnings of damaging wind events.

The collocated increase in  $Z_{DR}$  occurs because evaporation tends to increase the median drop size. For a given drop size distribution, the median drop size increases when the smaller drops are truncated. This truncation can occur via size sorting or through evaporation. In a stratiform region of a MCS, size sorting mechanisms are unlikely as the conditions in the storm are relatively quiescent (compared to the convective region). Thus, it seems probable that the increase in median drop size and the accordant increase in  $Z_{DR}$  can be attributed to evaporation. Melting graupel is also unlikely in this part of the storm since the increase in  $Z_{DR}$  is found well below the melting layer of the stratiform precipitation region.

At S band in pure rain,  $\rho_{HV}$  does not decrease substantially, generally remaining above about 0.98. Thus, changes in the drop size distribution due to evaporation do not significantly change  $\rho_{HV}$ . Nonetheless,  $\rho_{HV}$  is quite useful in detecting the melting layer (e.g., Giangrande et al. 2008; Brandes and Ikeda 2004) which is generally the level where the RIJ forms. Thus, identifying the melting layer is important for allowing forecasters to identify regions where the RIJ may become evident in the other polarimetric variables. The effect of evaporation on  $\rho_{HV}$  at C band will be more pronounced due to the stronger resonance scattering effects present at smaller wavelengths. The truncation of the DSD will cause  $\rho_{HV}$  to decrease for most drop size distributions, anticorrelated with the increase in  $Z_{DR}$ . This effect is quantified by a simple bin microphysics model of evaporation presented in Kumjian and Ryzhkov (2008).

#### 4. SUMMARY AND CONCLUSIONS

For the first time a polarimetric WSR-88D is used to collect data of a severe MCS with rapid update times. Operationally, the WSR-88D is not used to collect rapid scan data; however, this study has shown that such a radar is capable of rapid scanning, proving more versatile than generally thought. The data were collected with a sector scan, with an update time about the same as the Phased Array Radar. However, the data are finer resolution spatially and have polarization diversity. Dual-polarization data provide important insight into storm microphysics, especially regarding processes such as melting and evaporation associated with the rear inflow of dry air.

The case presented in this study exemplifies the operational applicability of polarimetric data for short-term forecasts of severe convective storms. The following conclusions can be drawn from this paper:

- (1) The development of the RIJ is associated with a decrease in  $Z_H$ ,  $K_{DP}$ , and an accordant increase in  $Z_{DR}$ .
- (2)  $K_{DP}$  may be most useful in first diagnosing the RIJ notch as it is more sensitive than  $Z_H$  to the smaller drops

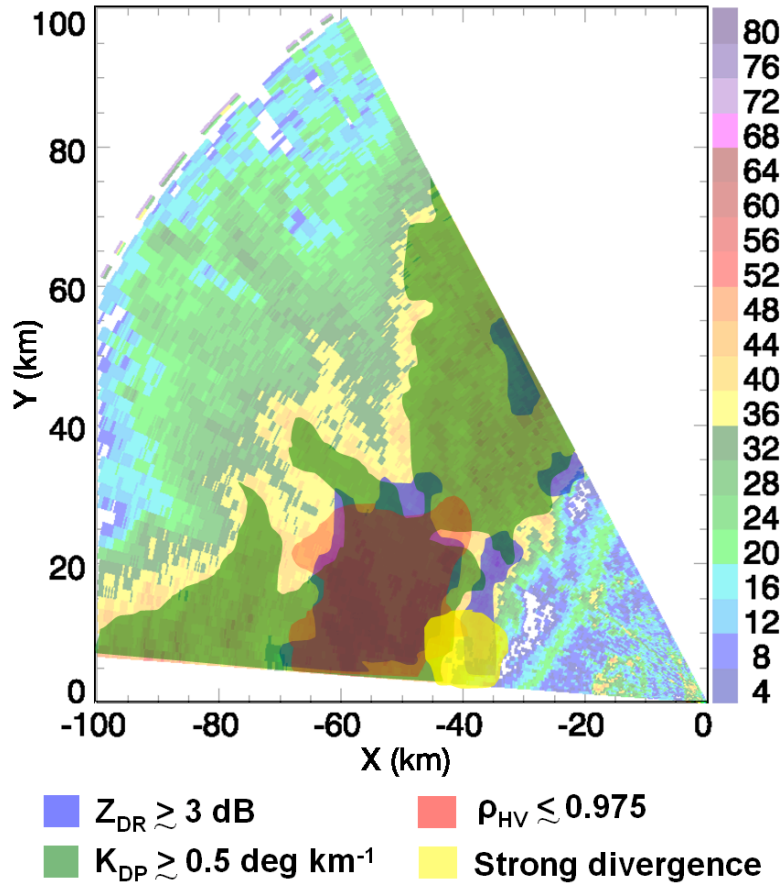


Fig. 5: Polarimetric variables overlaid on the observed  $Z_H$  field from 0649:04 UTC, from the 0.8° elevation angle. The bluish shading represents a region with  $Z_{DR}$  greater than about 3 dB, the green shading for  $K_{DP}$  greater than about 0.5 deg km<sup>-1</sup>, the red shading for an area of low  $\rho_{HV}$ , and the yellow highlights the divergence in the Doppler velocity field.

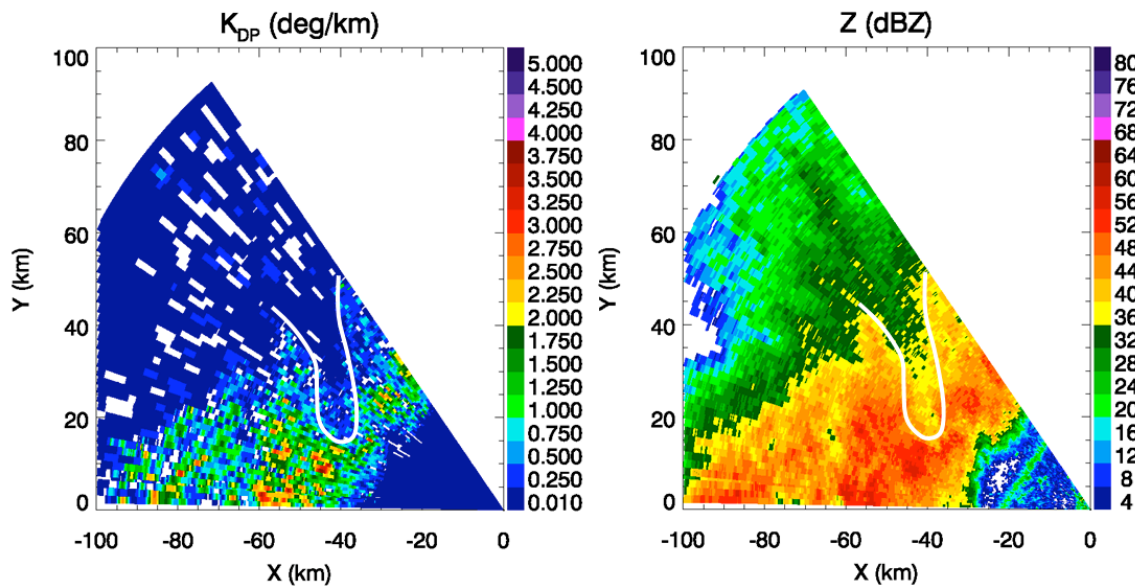


Fig. 6: Fields of  $K_{DP}$  (left) and  $Z_H$  (right) at 0656:59 UTC. The white line outlines the region of erosion in  $K_{DP}$  and is overlaid on  $Z_H$ . The slight erosion of  $Z_H$  is less evident than the  $K_{DP}$  erosion, which is more responsive to the evaporation of smaller drops.

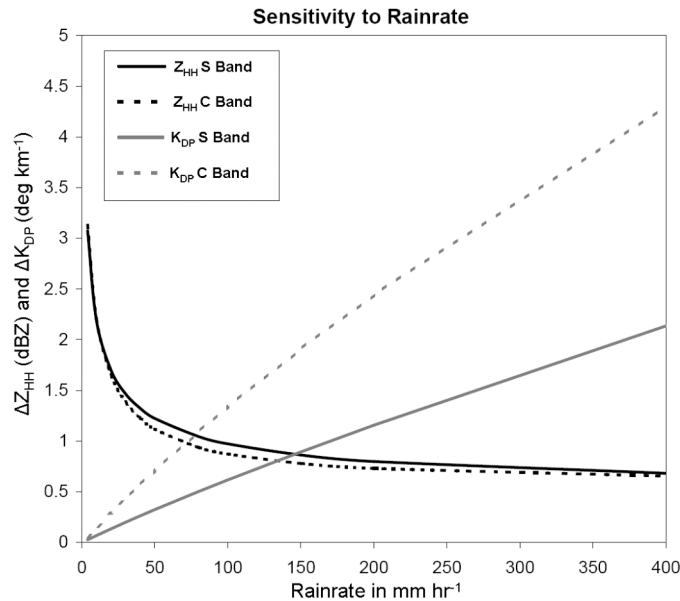


Fig. 7: Results of a simple model depicting the sensitivity of changes in polarimetric variables  $Z_H$  (black) and  $K_{DP}$  (gray) to rainfall rate at S band (solid) and C band (dashed) due to evaporation of raindrops. The changes occur over a 3 km depth in an environment with a dry adiabatic lapse rate and constant 75% relative humidity, assuming an initial Marshall-Palmer drop size distribution. Adapted from Kumjian and Ryzhkov (2008).

that are preferentially evaporated by the influx of dry midlevel air at the rear of the storm. The sensitivity of  $K_{DP}$  to evaporation increases for increasing rainfall rate while the sensitivity of  $Z_H$  decreases.

(3) The polarimetric variables display much more variability between scans than  $Z_H$ , illustrating the nonstationarity of such storms and highlighting the importance of rapid scan *polarimetric* data for operational forecasts, making a call for the development and implementation of polarization diversity for systems such as the Multifunction Phased Array Radar (MPAR).

(4) Rapid scanning strategies are possible with WSR-88D radars, which are more versatile than previously thought. Such capabilities are extremely underused.

## 5. ACKNOWLEDGEMENTS

We would like to thank the NSSL/CIMMS employees and engineers who maintain KOUN at research-grade quality for data collection. Dr. Valery Melnikov helped develop and implemented the sector scan routine. Parital funding for this study comes from NSF Grant ATM-0532107 as well as NOAA/Univ. of Oklahoma Cooperative Agreement NA17RJ1227 under the U.S. Dept. of Commerce. We also acknowledge useful discussions with Dr. Terry Schuur.

## 6. REFERENCES

Biggerstaff, M.I., and R.A. Houze, 1991: Kinematic and precipitation structure of the 10–11 June 1985 squall line. *Mon. Wea. Rev.*, **119**, 3034–3065.

Bluestein, H.B., 1993: *Synoptic-Dynamic Meteorology in Midlatitudes. Volume II: Observations and Theory of Weather Systems*. Oxford University Press, 594 pp.

Brandes, E.A., and K. Ikeda, 2004: Freezing-level estimation with polarimetric radar. *J. Appl. Meteor.*, **43**, 1541–1553.

Fovell, R.G., and Y. Ogura, 1988: Numerical simulation of a midlatitude squall line in Two Dimensions. *J. Atmos. Sci.*, **45**, 3846–3879.

Giangrande, S.E., J.M. Krause, and A.V. Ryzhkov, 2008: Automatic designation of the melting layer with a polarimetric prototype of the WSR-88D radar. *J. Appl. Meteor. and Climatology*, **47**, 1354–1364.

Houze, R.A., 1993: *Cloud Dynamics*. Academic Press, 573 pp.

Houze, R.A., M. Biggerstaff, S. Rutledge, and B. Smull, 1989: Interpretation of Doppler weather radar displays of midlatitude mesoscale convective systems. *Bull. Amer. Meteor. Soc.*, **70**, 608–619.

Kumjian, M.R. and A.V. Ryzhkov, 2008: Microphysical differences between tornadic and nontornadic supercell rear-flank downdrafts revealed by dual-polarization radar measurements. Extended Abstracts, 24<sup>th</sup> Conf. Severe Local Storms, Savannah, GA, Amer. Meteor. Soc., 3B.4.

Kumjian, M.R. and A.V. Ryzhkov, 2009: Storm-relative helicity revealed from polarimetric radar measurements. *J. Atmos. Sci.*, **in press**.

Lafore, J.P., and M.W. Moncrieff, 1989: A numerical investigation of the organization and interaction of the convective and stratiform regions of tropical squall lines. *J. Atmos. Sci.*, **46**, 521–544.

Meischner, P., V. Bringi, D. Heimann, and H. Höller, 1991: A squall line in southern Germany: Kinematics and precipitation formation as deduced by advanced polarimetric and Doppler radar measurements. *Mon. Wea. Rev.*, **119**, 678–701.

Ryzhkov, A.V., and D. Zrníc, 1994: Precipitation observed in Oklahoma mesoscale convective systems with a polarimetric radar. *J. Appl. Meteor.*, **33**, 455–464.

Schuur, T.J., W.D. Rust, B.F. Smull, and T.C. Marshall, 1991: Electrical and kinematic structure of the stratiform precipitation region trailing an Oklahoma squall line. *J. Atmos. Sci.*, **48**, 825–842.

Smull, B.F., and R.A. Houze, 1987: Rear inflow in squall lines with trailing stratiform precipitation. *Mon. Wea. Rev.*, **115**, 2869–2889.

Weisman, M.L., 1992: The role of convectively generated rear-inflow jets in the evolution of long-lived mesoconvective systems. *J. Atmos. Sci.*, **49**, 1826–1847.

Zrníc, D., N. Balakrishnan, C. Ziegler, V. Bringi, K. Aydin, and T. Matejka, 1993: Polarimetric signatures in the stratiform region of a mesoscale convective system. *J. Appl. Meteor.*, **32**, 678–693.